Chemical Geology 524 (2019) 174–183

Contents lists available at ScienceDirect

Chemical Geology

journal homepage: www.elsevier.com/locate/chemgeo

# Past and current geochemical conditions influence silicon isotope signatures of pedogenic clay minerals at the soil profile scale, Ethiopia

J.-T. Cornelis[a,b,c,*], D. Weis[a], S. Opfergelt[c], E. Van Ranst[d], M. Dumon[d]

[a] Pacific Centre for Isotopic and Geochemical Research, Department of Earth, Ocean and Atmospheric Sciences, University of British Columbia (UBC), 6339 Stores Road, Vancouver BC-V6T 1Z4, Canada
[b] TERRA Teaching and Research Centre, Gembloux Agro-Bio Tech, University of Liege, 5030 Gembloux, Belgium
[c] Earth and Life Institute - Environmental Sciences, Université Catholique de Louvain, Croix du Sud 2/10, B-1348 Louvain-la-Neuve, Belgium
[d] Department of Geology (WE13), Ghent University, Krijgslaan 281/S8, B-9000 Gent, Belgium

ARTICLE INFO

Editor: Jérôme Gaillardet

*Keywords:*
Soil formation
Clay minerals
Si isotopes
Inheritance
Neoformation
Weathering solution

ABSTRACT

Soil processes strongly govern silicon (Si) mobility in terrestrial environments and its relation to other global biogeochemical cycles. The nature of inherited soil clay minerals can be highly diverse given the variability of their weathering environment. The influence of Si isotope fractionation factor in the initial geochemical conditions of clay precipitation can therefore be still expressed in inherited clay minerals in their new environment. We studied top- and subsoil of an Ethiopian Vertic Planosol derived from parent materials of similar sources of volcanism. The selected Planosol has an abrupt textural change at a depth of ~40 cm separating a bleached, silty (25 ± 1.8% clay) ash-derived soil horizon with a crumby structure from a heavy clayey (68 ± 3.4% clay) lacustrine-derived vertic soil horizon. The mineralogical assemblage of the clay fraction in top- and subsoil is characterized by similar proportions of 1:1 (kaolinite) and 2:1 (illite and smectite) layer-type clay minerals. This specific soil profile provides a unique opportunity to elucidate the influence of clay formation processes (inheritance versus neoformation) on the Si isotope signature of pedogenic clay minerals. Minerals of the clay fraction in the clayey vertic horizon are significantly enriched in light Si isotope ($\delta^{30}Si = -1.41 \pm 0.02‰$) compared to the bleached, silty horizon ($\delta^{30}Si = -0.69 \pm 0.03‰$). These results are corroborated by the preferential enrichment in Ge, relative to Si, in the clay fraction of the clayey subsoil compared to the silty topsoil ($Ge/Si = 6.3 \pm 0.14$ and $4.0 \pm 0.10\ \mu mol\ mol^{-1}$, respectively). Our results demonstrate that geochemical conditions in lacustrine environment favor kinetically-driven Si isotope fractionation factor leading to lower Si isotope ratios in 2:1 clay minerals inherited in the new soil profile environment. The inherited soil textural conditions in the soil profile also contribute to on-going processes that result in larger Si isotope differences between the soil solution ($CaCl_2$ extractable) and clay minerals. This implies that Si isotope signatures of clay minerals in the studied soil profile are influenced by a combination of inheritance processes in lacustrine environment and on-going neoformation processes in the soil profile. This finding has important implications for environmental studies using geochemical and Si stable isotope tracers to better understand current soil processes, to model elemental cycling in soil-plant systems and to quantify land-ocean element mass-balances.

## 1. Introduction

Soil biogeochemical processes control stocks and fluxes of elements in terrestrial ecosystems and need therefore to be understood for (i) optimizing cycling of nutrients in ecosystems affected by anthropogenic activities, and (ii) assessing the interconnections between biogeochemical cycling of elements in terrestrial ecosystems. Despite important progress made in modeling and its cross-validation by empirical tests (Urey, 1947; Bouchez et al., 2013), the vast number and complexity of environmental parameters controlling soil-forming processes make their understanding difficult, especially for their impact on the cycling of elements. Soil physico-chemical and mineralogical characterizations, together with geochemical and isotopic analyses help to better assess the origin of processes that govern the formation of organic and inorganic phases in soils and its resulting effects on biogeochemical balance of elements (Chadwick and Chorover, 2001). In this

* Corresponding author at: TERRA Teaching and Research Centre, Water-Soil-Plant Exchanges, Gembloux Agro-Bio Tech, University of Liege (ULiège), 5030 Gembloux, Belgium.
*E-mail address:* jtcornelis@uliege.be (J.-T. Cornelis).

https://doi.org/10.1016/j.chemgeo.2019.06.013
Received 3 September 2018; Received in revised form 10 May 2019; Accepted 10 June 2019
Available online 11 June 2019
0009-2541/ 

regard, the extent of stable isotope fractionation between dissolved and solid phases (Si, Fe, Mg, Li) occurring in natural soil environments is regarded as a promising proxy to trace element pathways in terrestrial environments (Poitrasson et al., 2008; Reynolds, 2011; Pogge von Strandmann et al., 2012; Oelze et al., 2014; Opfergelt et al., 2017a). The relative enrichment in Ge (relative to Si) and light Si isotope ($^{28}$Si relative to $^{30}$Si) of secondary clay minerals allows to trace pedogenic processes through the soil profile and their resulting influence on biocycling of Si in terrestrial ecosystems and Si transfer from land to ocean (Ziegler et al., 2005; Cornelis et al., 2011; Opfergelt and Delmelle, 2012; Vandevenne et al., 2015; Frings et al., 2016; Opfergelt et al., 2017b).

When used in combination with Ge/Si elemental ratio, the stable Si isotope ratio provides a very powerful geochemical tracer of Si pathways in soil-plant systems (Opfergelt et al., 2010; Cornelis et al., 2010). The precipitation of secondary clay minerals, which preferentially incorporate light Si isotopes relative to soil solution (low $\delta^{30}$Si value) (Ziegler et al., 2005; Georg et al., 2007; Opfergelt et al., 2010), depletes the soil solution in light Si isotope (high $\delta^{30}$Si value) compared to the soil parent material (Cardinal et al., 2010; Cornelis et al., 2010). Silicon isotope analyses need therefore to be combined with those of Ge/Si ratios (Froelich and Andreae, 1981) as biogenic Si precipitates in plants (phytoliths) and incorporates stable Si isotopes with a large range of isotopic fractionation (Reynolds, 2011; Cornelis et al., 2011; Opfergelt and Delmelle, 2012; Frings et al., 2016). Precipitation of secondary clay minerals preferentially concentrates Ge (high Ge/Si) compared to phytoliths which do not incorporate Ge (low Ge/Si) (Kurtz et al., 2002; Derry et al., 2005; Lugolobi et al., 2010; Opfergelt et al., 2010). The Si stable isotope fractionation in soils is controlled by rock weathering/soil formation processes (Si precipitation/adsorption), resulting in a specific Si isotope signature of soils. Soil desilication, increasing with the degree of soil weathering (Si loss by leaching), affects Si isotope signatures of clay minerals (Basile-Doelsch et al., 2005; Ziegler et al., 2005; Opfergelt et al., 2011, 2012; Steinhoefel et al., 2011; Cornelis et al., 2014a; Ameijeiras-Mariño et al., 2017). The soil desilication implies formation of 1:1 clay minerals (kaolinite-type) enriched in light Si isotope (lower $\delta^{30}$Si value: −2.2‰), while 2:1 minerals are relatively less enriched in light Si isotope (higher $\delta^{30}$Si value: −0.16 to −0.52‰) (e.g., Ziegler et al., 2005; Georg et al., 2009; Opfergelt et al., 2010). In soil weathering sequence characterized by increasing annual rainfall, clay-sized minerals have lower Si isotope ratios in high precipitation areas (Si depletion) relative to the clay-sized minerals in low precipitation areas (Bern et al., 2010; Opfergelt et al., 2012). This highlights the importance to better understand soil-forming processes controlling Si isotope fractionation in natural environments. The residence time of the soil weathering solution largely depends on topographic situation, soil texture, structure, porosity and resulting permeability conditions (Lasaga, 1984; Berner, 1978; Maher, 2010). This soil property has never been taken into account when studying Si isotope fractionation during clay mineral formation in natural soil environments, while geochemical equilibria in solid-water interfaces are strongly controlled by the chemistry and residence time of the soil solution (Sverdrup, 1996). It is therefore especially important to study the influence of contrasting geochemical conditions on Si isotope fractionation during the formation of pedogenic clay minerals given that solid-water silicon isotope fractionation is essentially kinetically driven as a function of the precipitation rate of Si solid phases (Geilert et al., 2015), as well temperature and pH conditions (Stamm et al., 2019). This system-dependent feature is mainly controlled by original Si concentration in solution (Oelze et al., 2014), concentration of Fe and Al hydroxide precursors (Oelze et al., 2015), and temperature and pH of the solid-water interface (Geilert et al., 2014; Stamm et al., 2019) during the kinetically-dominated first step of precipitation (Roerdink et al., 2015). To understand the role of initial geochemical conditions on Si stable isotope fractionation, we analyzed Si isotope and Ge/Si ratios in soil solution, bulk soil, clay and silt fractions of a unique soil profile, an Ethiopian Vertic Planosol, characterized by the presence of a bleached, silty ash-derived soil horizon (with 25, 71, and 4% clay, silt and sand, respectively) that abruptly overlays a heavy clayey lacustrine-derived vertic horizon (with 68, 26 and 6% clay, silt and sand, respectively). Both horizons formed from similar parent material but at different geological time and under different geochemical conditions (ash-layer deposit for the silty horizon and lacustrine deposit for the vertic horizon). We relate the Si isotope composition and Ge/Si ratios of clay-sized minerals to the clay mineralogy of the two soil horizons as quantified by Dumon et al. (2014). The selected study site represents an almost perfect opportunity to assess the influence of past and current geochemical conditions on Si isotope signature of pedogenic clay minerals. The textural and permeability differences between the two environments (ash-derived and lacustrine-derived soil horizons) imply contrasting residence time of weathering solution that can affect Si isotope fractionation factor during formation of pedogenic clay minerals. The studied site allow to compare Si isotope signature of 1:1 and 2:1 clay minerals formed in contrasting geochemical conditions (Cornelis et al., 2014a), but originated from parent material of similar sources of volcanism (Van Ranst et al., 2011; Dumon et al., 2014).

## 2. Materials and methods

### 2.1. Study site

The Gilgel-Gibe catchment in south-western Ethiopia covers an area of about 5500 km$^2$ and is located near Jimma in the Kefa zone about 260 km of Addis Ababa (latitude 7° 22′72″ - 7° 34′84′ N; longitude 37° 21′05″ - 37° 28′80″ E). The geological complex basement was uplifted during the Upper Eocene as part of the Arabo-Ethiopian swell, which gave rise to the East-African rift system (Tadesse et al., 2003). The bedrock is characterized by rhyolite cross-cut by andesite and trachyte, columnar basaltic lavas (hawaiite) with tuff and lacustrine intercalations. The study area is mountainous (1096 to 3259 m a.s.l.) and characterized by steeply incising, V-shaped river valleys in the catchment flanks and a less pronounced stepped landscape of consecutive terraces at the centre of the catchment close to the Omo-River basin. The climate of the Gilgel Gibe area is sub-humid. Rain mostly falls between May and September. The mean annual rainfall in the catchment increases from 1300 mm in the lower valley areas to 2000 mm in the highest regions. Temperature is fairly constant throughout the year, with the mean minimum, maximum and average temperatures at 1800 mm altitude (Jimma station) being 11 °C, 25 °C and 17 °C, respectively. Most land is under cultivation (63.4%) and the remaining woodland (8.8%) is steadily being invaded by cultures. The main crop grown in the sampling area is teff (*Eragrostis abyssinica* (Jacq.)). The major reference soil groups in the catchment are Nitisols, Acrisols, Ferralsols, Vertisols and Planosols (Van Ranst et al., 2011). The soil selected for this study is a Vertic Planosol (IUSS Working Group WRB, 2015) located at the Bore-Waro test site in the middle of the lower terrace at some 200 m distance from the Gibe river, about 30 m above its present alluvial plain (Fig. 1). This typical Ethiopian Vertic Planosol presents a well rooted Ap horizon of 8–10 cm thick above a bleached dark grey (10YR 4-5/1, moist) to light grey (10YR 7/2, dry) silty (25 ± 1.8% clay) E horizon with a crumbly structure that at about a depth of 40 cm abruptly overlays a black (10YR 2/1, moist and dry) heavy clayey (68 ± 3.4% clay) vertic (Bi) horizon (Van Ranst et al., 2011). The soilscape at the study area is mainly used for grazing. The vertic Bi horizon is believed to be a lacustrine deposit, resulting from the weathering of the volcanic rocks making up the catchment. The bleached E horizon is a weathered ash layer deposited on top of this older sediment.

### 2.2. Soil sample collection and processing

Soil samples were collected at the following systematic depths (cm),

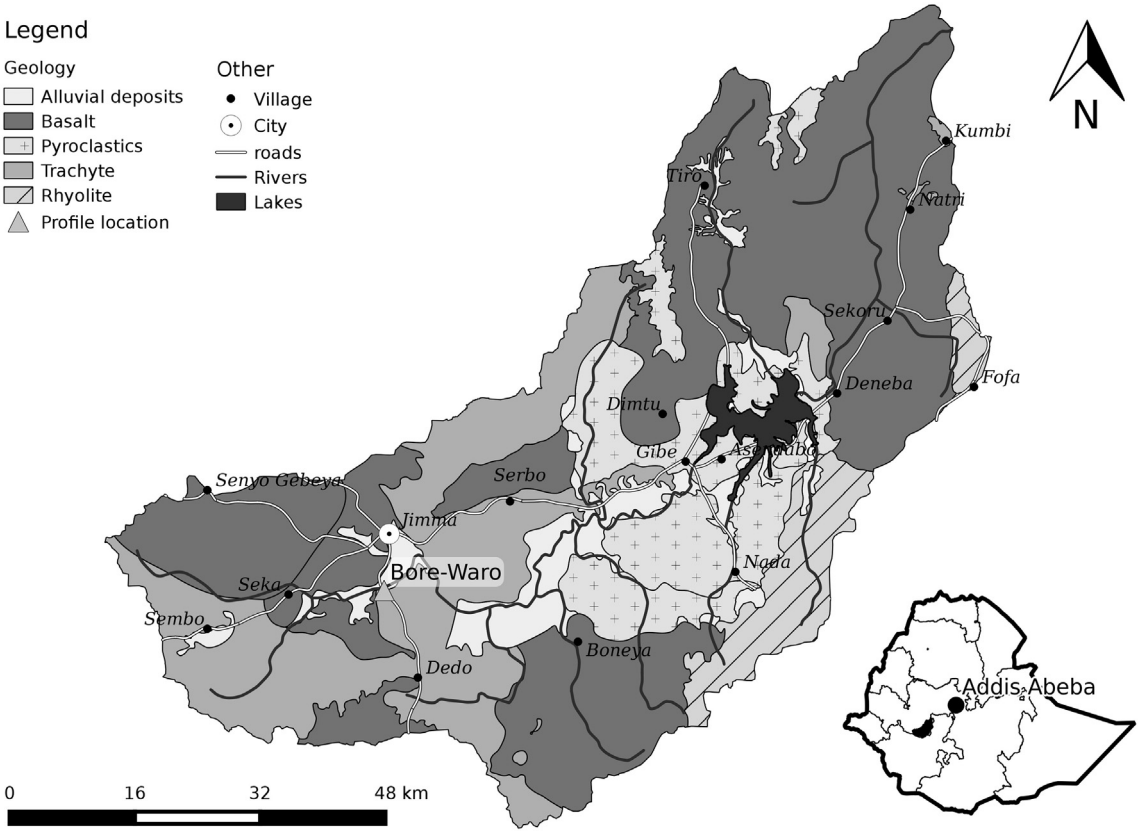


**Fig. 1.** Localization of the studied site on the geological map: the Bore-Waro profile (grey triangle) within the Gilgel-Gibe catchment (located in black in the inset) in Ethiopia.

with special attention to sampling at the transition between bleached and vertic horizons: 5–10 (Ap/E); 10–15; 15–20; 20–25; 25–30; 30–35 (E); 35–40 (Ecg); 40–45; 45–50; 50–55 and 70–75 (Bi). For the geochemical and isotopic analyses, the soil samples were gathered for the following horizons: Ap/E (surface horizon), E (bleached horizon) and Bi (vertic horizon). Composite samples of the major grass species were taken above and adjacent to the soil sampling area.

The particle size distribution (< 2 µm, 2–63 µm and 63–2000 µm) and main physico-chemical properties of air-dried fine earth (< 2 mm) are reported in Table 1. The sand fraction was separated from fine earth by ultrasonic dispersion and wet sieving. The clay fraction was separated from the silt fraction by dispersion with a solution of $Na_2CO_3$ at pH 9–9.5. After separation the clay is flocculated again at pH ± 6 with a solution of HCl and NaCl (Christensen, 1992). The recovered clay was thoroughly washed with alcohol to remove excess chloride, centrifuged at 3500 rpm after each step. The soil fractions were used for a detailed mineralogical characterization.

Oriented samples of $Ca^{2+}$-saturated clay fractions were prepared by transferring a suspension on glass slides. For each air-dried slide an X-ray diffraction (XRD) pattern was recorded before and after glycolation. These patterns have been designed using structural models optimized for each clay species present. More details on sample preparation, measuring conditions, interpretation and modeling can be found in Dumon et al. (2014). The silt fraction was micronized to a particle size < 10 µm using a McCrone micronizing mill, ethanol as grinding fluid and after addition of 5% ZnO as internal standard. The obtained slurries were then spray-dried (Kleeberg et al., 2008) after which an XRD pattern was recorded. The XRD patterns were quantified using the

**Table 1**
Physico-chemical characteristics of the fine earth of the different horizons of the Borè soil profile (Van Ranst et al., 2011). OC = organic carbon, CEC = cation exchange capacity, base saturation = ratio of the [sum of exchangeable Ca + Mg + K + Na]/CEC.

| Horizon | Depth (cm) | Clay | Silt | Sand | | $pH_{H2O}$ | Exchangeable complex ($cmol_c kg^{-1}$) | | | | | Base saturation |
|---|---|---|---|---|---|---|---|---|---|---|---|---|
| | | < 2 µm | 2–63 µm | 63 µm–2 mm | $OC_{tot}$ | | CEC | Ca | Mg | K | Na | (%) |
| Ap/E | 5–10 | 27 | 69 | 4 | 3.08 | 5.2 | 20.7 | 6.0 | 1.2 | 0.7 | 0.2 | 38 |
| E | 10–15 | 27 | 69 | 4 | 1.90 | 5.3 | 16.1 | 5.0 | 0.9 | 0.2 | 0.2 | 40 |
| E | 15–20 | 26 | 70 | 4 | 1.35 | 5.2 | 13.0 | 4.0 | 0.9 | 0.1 | 0.2 | 38 |
| E | 20–25 | 24 | 72 | 4 | 0.82 | 5.1 | 10.0 | 3.3 | 0.7 | 0.1 | 0.2 | 43 |
| E | 25–30 | 23 | 73 | 4 | 0.58 | 5.3 | 8.8 | 3.4 | 0.7 | 0.1 | 0.2 | 51 |
| E | 30–35 | 23 | 73 | 4 | 0.51 | 5.6 | 8.8 | 4.3 | 0.8 | 0.1 | 0.3 | 62 |
| Ecg | 35–40 | 25 | 67 | 8 | 0.53 | 5.6 | 11.0 | 5.4 | 1.2 | 0.1 | 0.3 | 64 |
| Bi | 40–45 | 63 | 30 | 7 | 1.05 | 5.9 | 45.9 | 26.2 | 6.4 | 0.7 | 0.7 | 74 |
| Bi | 45–50 | 70 | 25 | 5 | 1.01 | 6.0 | 52.0 | 32.7 | 7.9 | 0.7 | 0.8 | 81 |
| Bi | 50–55 | 69 | 26 | 5 | 0.89 | 5.8 | 51.9 | 33.8 | 7.6 | 0.8 | 0.8 | 83 |
| Bi | 70–75 | 70 | 25 | 5 | 0.94 | 6.0 | 53.1 | 35.9 | 9.0 | 0.8 | 0.8 | 87 |

BGMN Rietveld model and using Profex as the user interface (Doebelin and Kleeberg, 2015). The amorphous material was quantified using a structure file calibrated with pure amorphous material separated from the samples, as described below (Scarlett and Madsen, 2006). The samples still contained some phyllosilicates which were modelled using an ordered kaolinite (Bish and Von Dreele, 1989) and a dioctahedral turbostratic smectite (Ufer et al., 2004) structure. The XRD patterns were collected on a Bruker D8 ECO advance equipped with a Cu anode X-ray tube and a position-sensitive, energy-dispersive LYNXEYE XE detector. Patterns were collected using a Bragg-Brentano θ-θ geometry from 3°2θ onwards.

The pool of so-called "plant-available Si" (Sauer et al., 2006), i.e. silicic acid in aqueous phase, was assessed by using a 0.01 M $CaCl_2$ extraction made from a 99% pure $CaCl_2$ powder. Here, the $CaCl_2$ extractable solution is assumed to represent soil solution. Five grams of equivalent soil dry weight was shaken with 50 ml of $CaCl_2$ solution for 5 h at 20 °C. The suspension was then centrifuged at 3000 rpm for 10 min and the supernatant filtered through Wathman no.2 paper.

For the extraction of phytoliths from grasses, i.e. phytogenic silica (PhSi), plant samples were washed successively with de-ionized water, HCl 1 M, ethanol 70% and rinsed again with de-ionized water in order to avoid dust and aeolian contaminations (Kelly, 1990). The grass samples dried overnight at 40 °C were grinded and digested at 120 °C in a concentrated $HNO_3$ (70%)/$H_2O_2$ (30%) mixture until the reaction ceased. The PhSi was filtered through a pre-weighed Whatman membrane 0.2 µm filter and rinsed with de-ionized water.

In soil, the amorphous silica particles with a density below 2.3 g $cm^{-3}$ (mainly PhSi; Cornelis et al., 2014b) were separated from the silt fraction (2–63 µm) following the heavy liquid method adapted from Kelly (1990). About 40 $cm^3$ of a zinc bromide solution ($ZnBr_2$, density = 2.3 g $cm^{-3}$) was added to 0.5 *g* of silt fraction and centrifuged at 4000 rpm for 10 min as described in Cornelis et al. (2010). The supernatant containing the floating material was carefully removed with a pipette and filtered through a pre-weighed 2.0 µm Teflon filter (PTFE), then rinsed with HCl 1 M and de-ionized water. The operation was repeated until negligible material is obtained (Herbauts et al., 1994).

The silt and sand fractions were examined using a petrographic microscope in plane polarized light (PPL) and crossed polarizers (XPL) after mounting the samples on a glass slide using glycerol. The magnetically less- and more-susceptible minerals of the coarser sand fraction (100–2000 µm) were separated by means of a magneto-separator using a current of 0.5 A (Cornelis et al., 2014b).

### 2.3. Analytical techniques for Ge/Si and Si isotope measurements

#### 2.3.1. Reagents and standards

All dissolutions and chemical separations were carried out in Class 100 laminar flow hoods in the Class 1000 clean labs and the mass spectrometric analyses were performed in Class 10,000 labs at the Pacific Centre for Isotopic and Geochemical Research (PCIGR) at the University of British Columbia. All reagents used were purified in-house by sub-boiling distillation in Teflon® Savillex bottles. All dilutions, rinses and cleanings were made using doubly de-ionized water (DDW) at 18 Ωcm$^{-1}$. The bottles, tubes and Savillex® used for chemistry and MC-ICP-MS analyses were cleaned prior to each use in hot (70 °C) alkaline cleanser (extran® 300) for 2 days, followed by 1 day in hot concentrated reagent grade HCl, 1 day in hot concentrated $HNO_3$ and then by final rinsing five times in cold DDW. Savillex® PFA vials used to collect purified Si samples were cleaned in an additional step with HF 10%/$HNO_3$ 50% *v*/v. Accuracy and reproducibility were checked for (i) $\delta^{30}$Si over a period of 7 months on the silica standard NBS-28, used as the international 'zero-point' reference material, and (ii) on a daily basis by analyses of secondary reference material diatomite (prepared and distributed by M. Brzezinski, University of California Santa Barbara) and USGS rock standard BHVO-2, and (2) for Ge on USGS rock standard AGV-1 and BCR-1.

#### 2.3.2. Sample digestion

Silicon isotope composition and Ge/Si ratios were measured on bulk soil, silt and clay fractions, phytoliths (PhSi), amorphous silica from silt fraction (ASi) and $CaCl_2$-extractable soil solutions from the bleached (E) and vertic (Bi) horizons.

An alkaline digestion with 99.99% pure NaOH was used to transform soil and phytolith samples into an aqueous HF-free solution. Solid soil samples were ground using a Si-free alumina (99.5%) mortar and pestle. Between 5 and 10 mg of the powdered samples were weighted out into Ag crucibles (made in-house from 99.9985% pure Ag sheet and rod) in which one pellet of NaOH flux (~120 mg) was added. The Ag crucibles were covered with an Ag sheet and the fusion was carried out in a muffle furnace for 10 min at 720 °C. After slight cooling, the crucibles and the cover plates were transferred into Savillex® beakers containing 15 ml DDW, in which the fusion cake dissolved. The solutions were briefly agitated ultrasonically before being transferred into pre-cleaned HDPE bottles using PTFE funnels. The crucibles and Savillex® beakers were rinsed three times to ensure the complete transfer of the fusion cake. Solutions were then acidified by adding 1.2 ml of concentrated $HNO_3$ (14 N), for 120 mg NaOH flux (Georg et al., 2006). The recovery of Si for the fusion procedure of standard (NBS-28) and reference materials (BHVO-2 and diatomite) was 99.0 ± 1.8% (1SD, $n = 9$), which is in good agreement with the 99.4 ± 2.6% recovery of Georg et al. (2006).

#### 2.3.3. Si measurement by ICP-OES

Si contents were analyzed directly in the solution from NaOH fusion and $CaCl_2$ extraction by ICP-OES (Varian 725-ES) with europium as internal standard. The accuracy was checked on reference BHVO-2 material. Our result on BHVO-2 (23.12 ± 0.69%, 2SD, $n = 6$) was in good agreement with the recommended value (23.3 ± 0.60%) provided by USGS (Wilson, 1997). Precision for 6 replicates of BHVO-2 on three different sessions of analysis was 1.5% RSD. Detection limit, determined by measuring the standard deviation on 4 total procedural blanks, was 100 ppb.

#### 2.3.4. Silicon separation chemistry

The cation exchange chromatography procedure used to isolate Si follows the method of Georg et al. (2006). Three duplicates of fusion of NBS-28, BHVO-2 and diatomite were used to check for Si yields during the chemical purification and for accuracy of Si isotopic compositions. The soil solution samples extracted with $CaCl_2$ were purified, as dissolved samples from fusion, through a cation exchange resin (BioRad AG50W-X12) filled to a 1.8 ml resin bed in BioRad columns (Georg et al., 2006). Before loading and purifying samples, the resin was cleaned in the column with 3 N HCl, 6 N HCl, 7 N $HNO_3$, 10 N HCl, 6 N HCl, 3 N HCl and then rinsed three times with DDW until a pH of 5.5 is reached. The Si eluate were collected in Savillex® PFA vials. The Si concentrations in the total procedural blanks from columns (i.e., 3 blanks from NaOH-fusion loaded in three different purification columns) were negligible (below the detection limit of ICP-OES, 100 ppb). For a Si loading between 2 and 200 µg in the eluate solution, the Si recovery was 100% after three rinses with 1 ml DDW. Before loading, the samples were diluted to 20 ppm, by applying exactly the same elution volumes for all samples. The elute sample volume was 2 ml, and then diluted to 5 ml by adding three times a DDW elution volume of 1 ml. The final Si concentration (8 ppm) in the purified solution was checked by ICP-OES, as well as Na and Ca concentrations (that were below the detection limit) to check the purity of the final solution. The amount of Si used (40 µg) is approximately ten times higher than the 3.6 µg load used for Si isotopes analyses using the high resolution capacity of the Nu Plasma 1700 (ETH Zürich) (Georg et al., 2006), but seven times lower than the 300 µg load used for the anion exchange chromatography (Engström et al., 2006). The Si recovery of the column

purification, monitored using standard and reference materials in order to avoid isotopic fractionation associated with chromatographic separation, is 100.4 ± 2.9 ( ± 1SD, $n$ = 31), which is close to the value of Georg et al. (2006): 100.1 ± 1.6%.

#### 2.3.5. Si isotope measurement by MC-ICP-MS

Silicon isotope compositions were measured on a Nu Plasma (Nu 021; Nu Instruments Ltd., UK) multi-collector inductively coupled plasma mass spectrometer (MC-ICP-MS) in dry plasma mode (cones of type B; Nu instruments) using a Cetac Aridus II desolvating device and an external Mg doping to correct mass bias in a $HNO_3$ matrix (Cardinal et al., 2003). The source slit was set to pseudo-high resolution (medium) mode and the collector slit was adjusted for each session in order to resolve polyatomic interferences of $^{14}N^{16}O$ on the $^{30}Si$ ion beam and of $^{14}N_2$ on the $^{28}Si$ ion beam (Abraham et al., 2008). After a washing of 3 min in $HNO_3$ 3% and 2 min in $HNO_3$ 0.2%, the instrumental blanks are < 15 mv using a PFA nebulizer with an uptake rate of 50–80 µl/min. One $\delta^{30}Si$-value is comprised of 25 cycles with 8 s integration time for each cycle with a 20s on-peak zero measurement before each analysis. The instrumental mass bias was corrected according to the standard-sample bracketing protocol, i.e. one sample measurement normalized to the average of two adjacent NBS-28 standard measurements. Silicon isotopic compositions are expressed as deviation of $^{30}Si/^{28}Si$ relative to the NBS-28 reference standard using the delta (δ) per mil (‰) notation as follows:

$$\delta^{30}Si = \left[ \frac{\left(\frac{^{30}Si}{^{28}Si}\right)_{sample}}{\left(\frac{^{30}Si}{^{28}Si}\right)_{NBS28}} - 1 \right] * 1000$$

Each sample was measured three times during at least two different analytical sessions. Silicon isotopic $\delta^{30}Si$-values are reported as the mean of replicate isotopic analyses (n = 3) ± 2 standard deviations (SD). The accuracy and reproducibility of the measurements were controlled by the measurement of (i) eight $\delta^{30}Si$-values of NBS-28 over 2 h before any analysis, and (ii) secondary reference materials (diatomite and BHVO-2) at the beginning and at the end of each sample series. The instrument sensitivity varies between 2 and 3.5 V/ppm Si at 0.1 ml/min uptake.

The reproducibility was checked over a period of 7 months (data were acquired during 4 sessions) on standard NBS-28 material: 0.01 ± 0.19‰ (2SD, $n$ = 45). This reproducibility also includes the repeatability of the protocol of fusion-dissolution-chromatography since the NBS-28 standards were processed through the chemical purification from different fusion procedures before each session. Accuracy and reproducibility on $\delta^{30}$ were also checked on reference materials during each session ensuring values similar to published values (Reynolds et al., 2007; Abraham et al., 2008; Georg et al., 2009; Opfergelt et al., 2011): 1.25 ± 0.15‰ (2SD, $n$ = 10) for diatomite and −0.29 ± 0.21‰ (2SD, $n$ = 5) for BHVO-2. We also checked the control of mass bias on $\delta^{30}Si$ and $\delta^{29}Si$ by ensuring that the measured $\delta^{30}Si$ values had an atomic mass unit difference between the $\delta^{30}$ and $\delta^{29}$ < 0.10.

#### 2.3.6. Ge chemistry and measurement by HR-ICP-MS

For Ge concentration measurements, the alkaline NaOH fusion was also performed on USGS rock standards AGV-1 and BCR-1. For soil and plant samples and USGS standards, aliquots of 5 g of the solution from the NaOH fusion were transferred into Savillex®, then dried at 120 °C overnight and subsequently re-dissolved in 3 ml 1% $v$/v $HNO_3$ spiked with 1 ng $g^{-1}$ In. The Savillex® beakers were capped and again placed on a hotplate at 120 °C for 10 min. The solutions were briefly ultrasonicated before their transfer into pre-cleaned HDPE bottles. The Savillex® beakers were rinsed and added to the HDPE bottles. The solutions were gravimetrically diluted 2 times to a weight of 10 g and Ge concentrations were determined by measurement of $^{74}Ge$ isotope directly on the HR-ICP-MS (Finnigan Element 2) in medium resolution.

Indium was used as the internal standard to correct for both instrumental (i.e., mass) drift, and sensitivity drift potentially arising from the sample matrix (Pretorius et al., 2006; Carpentier et al., 2013; Schudel et al., 2015). A total procedural blank was included with each batch of seven samples analyzed. The detection limit for Ge, checked by measuring the 2 standard deviations (2SD) on 6 procedural blanks of the NaOH fusion, was 1.6 ppb. Accuracy and reproducibility were also checked on reference materials during each session ensuring values nearly identical to the ones reported using isotope-dilution hydride-generation ICP-MS technique developed by Mortlock and Froelich (1996): BCR-1 = 1.52 ± 0.2 ppm (Kurtz et al., 2002), 1.59 ± 0.2 ppm (Scribner et al., 2006) and AGV-1 = 1.25 ± 0.1 ppm (value downloaded from GeoRem; Jochum et al., 2005). Our analysis of Ge in BCR-1 (1.64 ± 0.18 ppm, 2SD, $n$ = 7) and in AGV-1 (1.13 ± 0.17 ppm, 2SD, $n$ = 8) agrees within error to the published values. Reproducibility for 7 replicates of BIR-1 on two sessions was 6% relative standard deviation (RSD). Each sample was measured two times.

## 3. Results

### 3.1. Soil physico-chemical characteristics

The soil characteristics of the studied Vertic Planosol thoroughly described in Van Ranst et al. (2011) and Cornelis et al. (2014b) are presented in the Table 1. The abrupt textural change between bleached, silty (around 70% silt) E and the black, heavy clayey (around 70% clay) Bi horizons is also characterized by an increase in organic carbon content from 0.5 to 1.0% and especially an increase of the cation exchange capacity (CEC), from 11 to 46 cmol(+)/kg. Both of the horizons have a very small sand content (about 5%). The upper bleached soil horizon has much higher total $SiO_2$ (> 72%), $Na_2O$ (1.1–1.3%) and $K_2O$ (1.8–3.7%) contents compared to the clayey vertic subsoil (53–55% $SiO_2$, 0.4–0.5% $Na_2O$ and 1.1–1.4% $K_2O$), indicating the dominance of siliceous components and feldspars in the upper horizon. At the transition between the two horizons, the increase of $Al_2O_3$, CaO, MgO, and $H_2O$ (loss on ignition) contents are due to the dominance of smectitic minerals in the clay fraction of the vertic horizon (Van Ranst et al., 2011).

### 3.2. Microscopic observations

A high content of phytoliths and irregularly shaped amorphous fragments of volcanic glass was observed in the coarser (silt and sand) fractions of the bleached horizon. Given that phytoliths are also mainly silt-sized, one can assume that the magnetic susceptible amorphous fragments in the sand fraction are volcanic glass, which were not detected in the same fraction of the vertic horizon. Indeed, smaller fragments were found in the silt fraction of the vertic horizon. The microscopic analysis of the silt fraction having a density below 2.3 g $cm^{-3}$ revealed a composition dominated by phytoliths showing morphologies very similar to those of the phytoliths extracted from grasses (Van Ranst et al., 2011; Cornelis et al., 2014b).

The mineralogical composition of the sand fraction (> 100 µm) of the bleached and vertic horizons is not significantly different. The most abundant minerals in this fraction are magnetic non-susceptible quartz (78%) and feldspars (13%). The magnetic susceptible fraction consists mainly of colorless fragments of volcanic glass and represents 9% of the sand fraction.

### 3.3. Quantitative clay mineralogy

The studied Vertic Planosol presents a complex clay mineralogy. The clay fraction of the bleached E horizon is composed of a mixture of kaolinite and illite (> 0.2 µm) and smectite and kaolinite/smectite

**Table 2**
Absolute weight fractions of the different phyllosilicate layer-types within the bulk clay fraction and sub-fractions of the studied Planosol (based on data from Dumon et al. (2014)). The relative weight of a given mineral in each sub-fraction is given in parenthesis.

| Horizon | Layer types | < 0.05 μm | 0.2–2 μm | Bulk < 2 μm |
|---|---|---|---|---|
| | | /wt% | /wt% | /wt% |
| Bleached E horizon | Kaolinite | 18 (50%) | 17 (30%) | 35 (38%) |
| | Illite | 2 (5%) | 33 (59%) | 35 (38%) |
| | Smectite | 16 (45%) | 6 (11%) | 22 (24%) |
| | Total | 36 | 56 | 92[a] |
| Vertic Bi horizon | Kaolinite | 32 (40%) | 2 (25%) | 34 (39%) |
| | Illite | 3 (4%) | 5 (63%) | 8 (9%) |
| | Smectite | 44 (55%) | 1 (12%) | 45 (52%) |
| | Total | 79 | 8 | 87[a] |

[a] The material of the 0.05–0.2 μm sub-fraction was not analyzed, explaining the < 100% totals.

mixed-layers (< 0.05 μm), while the clay fraction of the vertic Bi horizon is dominated by a large amount of fine clay composed of smectite and kaolinite/smectite mixed-layers (< 0.05 μm). Despite higher content of fine clay in the bulk vertic horizon, the proportion of the different clay mineral species (kaolinite, illite and smectite) between E and Bi soil horizons is nearly identical in the clay sub-fractions (< 0.05 μm and 0.2–2 μm; Table 2) (Dumon et al., 2014). A quantitative composition of this complex mineralogy whereby only the amount of kaolinite, illite and smectite layers present in the different phases are considered and by disregarding the layer-stacking is given in Table 2 (from Dumon et al., 2014). The data illustrates that the fine clay fraction (< 0.05 μm) of both horizons is composed of dominantly kaolinite and smectite layer types in roughly the same proportion, with only minor amounts of illite layer types. The coarse clay fraction (2–0.2 μm) of both horizons is composed dominantly of illite layer types and to a lesser degree of kaolinite layer types. Only minor amounts of smectite layer types are present. The summation of the content of each clay mineral species of the two sub-fractions leads to the difference in mineralogy for the bulk (< 2 μm) clay fraction: E horizon more concentrated in illite and Bi horizon more concentrated in smectite. Based on X-ray characteristics (Dumon et al., 2014), illite is assumed not to be derived from primary rock-forming mica.

### 3.4. Quantitative silt-sized mineralogy

About 50% of the silt fraction is amorphous (volcanic glass and phytoliths), quartz makes up 22 to 30%, feldspars 11 to 18% and phyllosilicates 6 to 17% (Table 3). Given the broad 00l reflections in combination with a typical turbostratic hk0 band, we can assume the phyllosilicates present to have a similar origin to those present in the clay fraction (smectite and kaolinite type layers). Most likely these phyllosilicates are in fact clay-sized, but are either coating or attached to silt-sized particles. The composition of the silt fraction in the vertic horizon is comparable, but with lower amounts of amorphous material and higher amounts of phyllosilicates.

**Table 3**
Mineralogical composition (in wt%) of the silt fraction (2–63 μm) in the Borè soil profile as determined by Rietveld refinement.

| Horizon | E horizon | E horizon | E horizon | Bi horizon | Bi horizon |
|---|---|---|---|---|---|
| Depth (cm) | 10–15 | 20–25 | 30–35 | 45–50 | 70–75 |
| Amorphous | 55.6 | 52.6 | 49.2 | 39.4 | 41.3 |
| Quartz | 22.4 | 27.2 | 29.8 | 25.9 | 26.7 |
| Feldspars | 11.3 | 12.8 | 14.1 | 15.4 | 17.9 |
| Phyllosilicates | 10.4 | 6.7 | 6.1 | 16.7 | 12.9 |
| Anatase | < 1 | < 1 | < 1 | < 1 | < 1 |
| Hematite | < 1 | < 1 | < 1 | < 1 | < 1 |
| Goethite | < 1 | < 1 | < 1 | 1.8 | < 1 |

### 3.5. Ge/Si ratios in soil, plant and solutions

The Ge/Si ratio measured in PhSi extracted from grasses (phytoliths) is 0.3 ± 0.02 μmol mol$^{-1}$ (Table 4). Amorphous silica extracted from soil (phytoliths and volcanic glass) are characterized by the lowest Ge/Si ratios, 0.08 ± 0.01 μmol mol$^{-1}$ and 0.04 ± 0.01 μmol mol$^{-1}$, respectively, in E and Bi horizons. The Ge/Si ratios of bulk soil differed between the two horizons, with a lower value for E horizon (1.4 ± 0.06 μmol mol$^{-1}$) compared to Bi horizon (4.6 ± 0.12 μmol mol$^{-1}$). The silt fractions of E and Bi horizons displayed strictly identical Ge/Si ratios with a value of 0.8 ± 0.02 μmol mol$^{-1}$, while Ge/Si ratios of clay fractions varied between E and Bi horizons: 4.0 ± 0.10 μmol mol$^{-1}$ and 6.3 ± 0.14 μmol mol$^{-1}$, respectively. The Ge/Si ratios in $CaCl_2$-extractable solutions were identical in both horizons: 0.3 ± 0.20 μmol mol$^{-1}$.

### 3.6. Si isotope compositions in soil, plant and solutions

Phytoliths extracted from plants (BSi) displayed $\delta^{30}$Si values of 0.22 ± 0.05‰ (2SD, $n$ = 3). Amorphous silica particles extracted from soil (volcanic glass and phytoliths) are characterized by the highest $\delta^{30}$Si values: 1.56 ± 0.10‰ in E horizon and 1.87 ± 0.17‰ in Bi horizon. The $\delta^{30}$Si values of bulk soil differed between the two soil horizons: lower isotope ratios in Bi horizon (−0.57 ± 0.32‰) compared to E horizon (0.40 ± 0.18‰). This enrichment in light $^{28}$Si is also observed in the respective clay fractions: lower isotope ratios in Bi horizon (−1.41 ± 0.02‰) compared to E horizon (−0.69 ± 0.02‰). The Si isotopic signature of silt fractions is quite similar: 0.48 ± 0.29‰ in E horizon and 0.37 ± 0.32‰ in Bi horizon. The $CaCl_2$-extractable solutions are characterized by different $\delta^{30}$Si values: Bi horizon depleted in light $^{28}$Si (1.58 ± 0.16‰) compared to E horizon (0.12 ± 0.21‰).

## 4. Discussion

### 4.1. Evolution of soil mineralogy

The quantitative clay mineralogical composition allowed Dumon et al. (2014) to conclude that the parent material of both, bleached (weathered ash layer) and vertic (lacustrine deposit from the weathering of the volcanic rocks) horizons, must have been compositionally similar as their origin is from the same volcanic parent material. However the age of minerals formed and geochemical conditions controlling mineral formation in the two soil horizons are different; the lacustrine deposit being older with lower permeability relative to the ash layer deposited on top of it that is younger with higher permeability.

The observed differences in mineralogy of the bulk soil are for the most part the result of differences in the relative proportions of size fractions. The bleached E horizon is silty (71% of silt on average for the E horizon) while the vertic Bi horizon is clayey (68% clay on average for the Bi horizon). The mineralogy of the clay sub-fractions of both horizons is very similar, but differs in terms of relative proportions of the phases present in the bulk clay fraction (Table 2). Without taking into account the unanalyzed 0.05–0.2 μm sub-fraction, the proportion of kaolinite layer types in the clay fraction is identical between E and Bi horizons: 38% and 39%, respectively. Quantitative clay mineralogy

**Table 4**
Si and Ge concentrations, Ge/Si and $\delta^{30}Si$ in the bulk soil, clay and silt fractions, ASi from silt-sized fraction, phytoliths and $CaCl_2$-extractable soil solution in the Borè soil profile.

| | Si | Ge | Ge/Si | 2SD | $\delta^{30}Si$ | 2SD |
|---|---|---|---|---|---|---|
| | (mmol $g^{-1}$)[a] | (nmol $g^{-1}$) | (μmol $mol^{-1}$) | | ‰ | |
| Phytoliths (BSi) | 14.5 | 4.4 | 0.3 | 0.02 | 0.22 | 0.05 |
| Granite-type bedrock[b] | 12.6 | 32.1 | 2.5 | 0.08 | −0.23 | 0.15 |
| Bleached E horizon | | | | | | |
| Bulk soil | 13.0 | 18.0 | 1.4 | 0.06 | 0.40 | 0.18 |
| Silt | 14.1 | 11.1 | 0.8 | 0.02 | 0.48 | 0.29 |
| Clay | 11.3 | 44.9 | 4.0 | 0.10 | −0.69 | 0.03 |
| ASi | 15.8 | 1.3 | 0.08 | 0.01 | 1.56 | 0.10 |
| Soil solution (mmol $l^{-1}$) | 0.2 | 0.06 | 0.3 | nd | 0.12 | 0.21 |
| Vertic Bi horizon | | | | | | |
| Bulk soil | 10.1 | 45.9 | 4.6 | 0.12 | −0.57 | 0.32 |
| Silt | 13.6 | 11.0 | 0.8 | 0.02 | 0.37 | 0.32 |
| Clay | 9.4 | 59.1 | 6.3 | 0.14 | −1.41 | 0.02 |
| ASi | 16.0 | 0.7 | 0.04 | 0.01 | 1.87 | 0.17 |
| Soil solution (mmol $l^{-1}$) | 0.6 | 0.2 | 0.3 | 0.20 | 1.58 | 0.16 |

[a] Except for soil solution, for which the unit is mmol $l^{-1}$.
[b] Ge/Si ratio from Cornelis et al. (2010) and $\delta^{30}Si$ value from Savage et al. (2012) in granite-type unweathered bedrock. Ge/Si and $\delta^{30}Si$ data from granite can be used as the equivalent for rhyolite parent material.

highlights that pedogenesis in the fine-textured Bi horizon implies dissolution of illite-type layers (9% of the analyzed clay fraction) and neoformation of smectite-type layers (52% of the analyzed clay fraction), compared to the coarser-textured E horizon where illite-type layers are still present (38% of the analyzed clay fraction) and precipitation of smectite-type layers is less abundant (24% of the analyzed clay fraction). The fine-textured and older vertic soil material (Bi horizon) is therefore more concentrated in smectite resulting from illite dissolution and smectite precipitation than in the coarser-textured and younger bleached soil material (E horizon). However, the proportions of 1:1 (kaolinite) and 2:1 (illite and smectite) layer-type clay minerals are similar between topsoil E horizon and subsoil Bi horizon.

### 4.2. $\delta^{30}Si$ and Ge/Si ratios variations in soils

The silt-sized inorganic constituents, mainly amorphous silicates (volcanic glass and phytoliths), quartz and feldspars, are characterized by comparable Si isotopic and Ge/Si geochemical signatures in both horizons (Fig. 2). This indicates that the primary minerals (Table 3) might have a similar geological origin, even if the depositional process and age of the E and Bi soil materials are different. This means that initial isotopic and geochemical signatures of silt-sized inorganic constituents cannot explain the different Si isotope signature of clay minerals between soil horizons with respect to variable primary mineral sources.

Bulk Bi soil material is relatively enriched in light $^{28}Si$ and Ge compared to E soil material (Fig. 2). As the silt fraction and ASi have similar $\delta^{30}Si$ signatures, the lighter Si isotope composition in Bi soil material is explained by the significant higher content of clay-sized minerals. Indeed, the proportion of clay fraction in Bi horizon is higher and relatively more enriched in light $^{28}Si$ and Ge compared to clay-sized minerals in E horizon. The Si isotope difference between $CaCl_2$-extractable solution and clay fraction ($\Delta^{30}Si_{solution\text{-}clay}$) is larger in the Bi than in the E horizon (+2.99‰ for the Bi horizon and +0.81‰ for the E horizon). This indicates that the formation of clay minerals governs the $\delta^{30}Si$ and Ge/Si variations in bulk soil, but also in the $CaCl_2$-extractable solution. This also entails that for Bi horizon, greater depletion in light Si isotope in the $CaCl_2$-extractable solution relative to clay

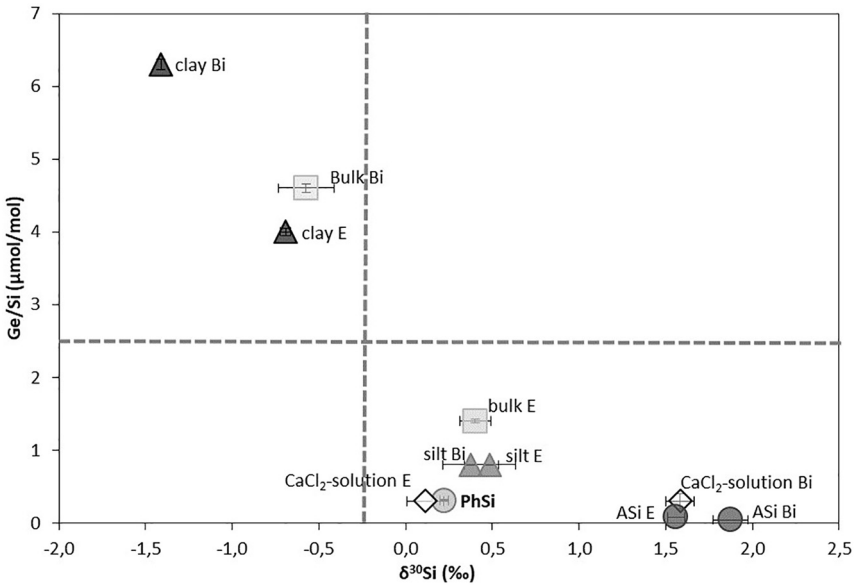


**Fig. 2.** Relationships between $\delta^{30}Si$ values and Ge/Si ratios in bulk soil (squares), clay fraction (black triangles), silt fraction (grey triangles), soil amorphous silica (ASi; grey circles) plant (PhSi; grey circle) and $CaCl_2$- extractable solution (diamonds). Dashed lines are the Si isotope and Ge/Si ratio signature of typical granite-type silicate rock signatures (Cornelis et al., 2010; Savage et al., 2012; Table 4).

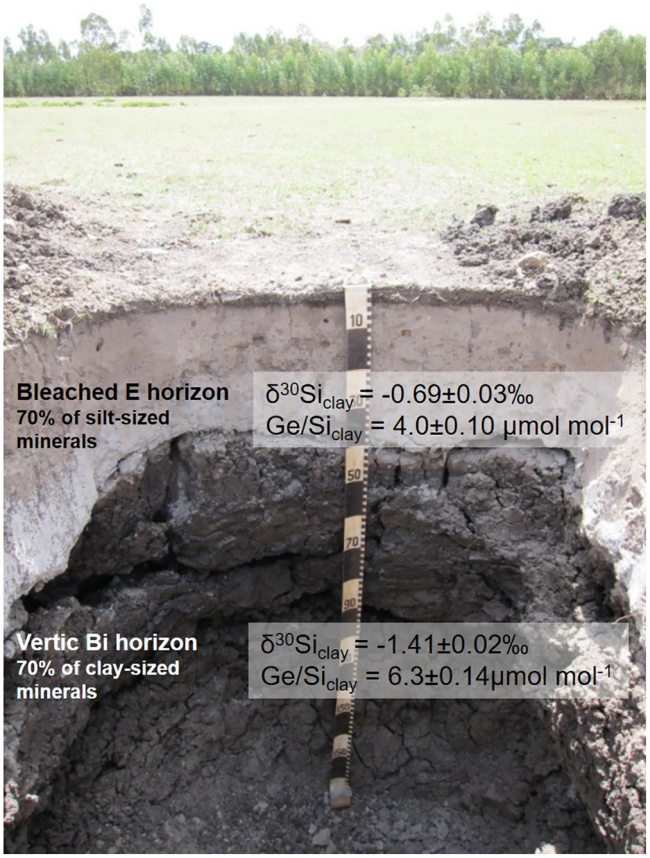


**Fig. 3.** Soil profile picture presenting the silty E horizon and clayey Bi horizon with their respective Si isotope signature and Ge/Si ratio in the clay fraction.

fraction is partly controlled by ongoing process affecting clay mineral formation/dissolution.

### *4.3. Geochemical conditions as a driver of solid-water interactions and resulting Si isotope signatures of pedogenic clay minerals*

The process of Si sorption onto Fe oxides must be investigated as it preferentially incorporates light Si isotopes (Delstanche et al., 2009). The dithionite-citrate-bicarbonate (DCB) selectively extracts free iron oxides in soils (Mehra and Jackson, 1960). DCB-extractable Si (1.2% in E horizon and 1.0% in Bi horizon) represents between 2.4 and 4.1% of total Si concentration in bulk soil and is not related to DCB-extractable Fe in the E (1.0%) and Bi (3.3%) horizons (Cornelis et al., 2014b). This means that the part of Si adsorbed onto Fe oxides does not substantially affect Si isotopic signature of the clay fraction compared to the process of Si precipitation in phyllosilicates (Delstanche et al., 2009; Opfergelt et al., 2010). The results of mineralogical, geochemical and isotope analyses indicate that the primary source of Si and the relative proportions of 1:1 (kaolinite) and 2:1 (illite and smectite) layer types in the clay fraction (Table 2) are comparable in the silty E horizon and in the clayey Bi horizon. Furthermore, it is well known that strongly desilicated soils, characterized by enrichment of 1:1 (kaolinite) layer types relative to 2:1 layer types, will present the lower Si isotope ratios (Ziegler et al., 2005; Opfergelt et al., 2012; Opfergelt and Delmelle, 2012). It is therefore surprising to observe lighter $\delta^{30}Si$ values in the clay fraction of Bi horizon compared to the clay fraction of E horizon for two soil horizons having similar proportions of 1:1 (kaolinite) and 2:1 (illite and smectite) layer types clay minerals. The Si isotope difference between solid and solution ($\Delta^{30}Si_{solid\text{-}solution}$) associated with primary mineral dissolution and precipitation of secondary phyllosilicate minerals is around +2‰ (Ziegler et al., 2005). However, the exact equilibrium and rate-dependent kinetic isotopic fractionations associated with dissolution/precipitation processes are still undetermined for 1:1 and 2:1 layer types clay minerals such as kaolinite, smectite and illite (Opfergelt and Delmelle, 2012; Frings et al., 2016). Given the lowest Si isotope ratio has been found in strongly desilicated soil enriched in kaolinite (Ziegler et al., 2005), we assume that the isotope fractionation factor associated with the dissolution of secondary illite minerals and precipitation of smectite minerals cannot explain such low $\delta^{30}Si$ values for the bulk clay fraction in the Bi horizon (−1.41‰) compared to E horizon (−0.69‰). The contrasting Si isotope and Ge/Si composition of the clay fraction between the Bi and E horizons cannot, therefore, only be explained by lower content of illite-type minerals in Bi compared to E horizon and the associated fractionation factor during dissolution-precipitation reactions.

The lower $\delta^{30}Si$ values and higher Ge/Si ratios in the clay fraction of the Bi horizon could be explained by different Si isotope fractionation factors between E and Bi horizons, i.e., different geochemical conditions favoring larger Si isotope fractionation during initial precipitation of clay minerals (kinetically-controlled fractionation) in one horizon relative to the other. In natural environments, the relative impact of equilibrium and kinetic isotope fractionation on Si isotope compositions measured are difficult to disentangle given that the equilibrium Si isotope fractionation factors between soil solution and solid phases are not known precisely. But kinetically-driven Si isotope fractionation factors are larger than Si isotope fractionation factors at equilibrium (Roerdink et al., 2015). The initial lacustrine environment of the Bi horizon is a confined area that concentrates the elements resulting in the accumulation of smectite-type minerals and formation of a vertic horizon in the current soil profile. The current higher Si concentration of $CaCl_2$-extractable solution in vertic Bi horizon (97.9 $mg.kg^{-1}$) relative to the bleached E horizon (21.8 $mg.kg^{-1}$; Cornelis et al., 2014b) confirms the confined area less affected by desilication. Our results suggest that in that confined lacustrine environment, the higher Si concentrations in solution favored kinetically-dominated Si isotope fractionation during Si adsorption onto Al-hydroxide precursors (Oelze et al., 2014) and preferentially adsorbing light Si isotopes. The secondary precipitates formed from these precursors inherited a light Si isotope composition (Oelze et al., 2014; Roerdink et al., 2015). The resulting lower Si isotope ratio in solid secondary products from that low permeability environment has been preserved in inherited secondary precipitates in the Bi horizon of the current soil profile (Fig. 3).

Regarding modern processes in this soil profile, permeability conditions, controlled by the contrasting textural properties, sharply differ between the ash-layer environment that is characterized by an intense leaching of pore water (E horizon), and the lacustrine-layer environment that is characterized by a much lower rate of water percolation (Bi horizon) (Van Ranst et al., 2011). Lower percolation rates in the Bi horizon than in the E horizon can lead to differences in Si isotope fractionation factors associated with on-going processes of clay formation in the two soil horizons, depending on the relative proportion of kinetic vs. equilibrium fractionation (Oelze et al., 2014; Roerdink et al., 2015). This is illustrated by the Si isotope difference between the clay fraction and the $CaCl_2$ solution ($\Delta^{30}Si_{solution\text{-}clay}$) in the two soil horizons: higher $\Delta^{30}Si_{solution\text{-}clay}$ in the vertic Bi horizon (−2.99‰) than in the bleached E horizon (−0.81‰). In specific soil conditions characterized by long residence time of pore water such as in the Bi horizon, the Si isotope composition of the soil solution ($CaCl_2$-extractable) reflects ongoing soil processes that may be kinetically-driven (with larger Si isotope fractionation factors; Roerdink et al., 2015) and lead to higher $\delta^{30}Si$ values in soil pore water of the Bi horizon (+1.58‰) compared to well-drained soil in E horizon (+0.12‰). In contrast in a well-drained soil environment such as the E horizon, pore water has lower ionic activity (lower Si concentration in $CaCl_2$-extractable solution) implying soil conditions less favorable to kinetically-driven Si isotope fractionation, and a resulting limited Si isotope fractionation factor (Roerdink et al., 2015).

The data highlights that residence time of pore water in soils is therefore a key factor that must be taken into account when using Si isotope signature of clay minerals to trace weathering processes.

### 4.4. Implications for tracing soil-forming processes using stable Si isotopes

Our study demonstrates that besides the known Si isotope fractionation factor associated with the dissolution of primary minerals and precipitation of secondary minerals, soil properties such as texture and permeability and resulting chemical composition of the solution must be taken into account when using Si isotope fractionation for tracing element pathways in water-soil-plant continuum.

Our results confirm that solid-water Si isotope fractionation associated with dissolution and precipitation of soil solid phases is system-dependent (Geilert et al., 2015). The different geochemical conditions likely drive solid-water interactions involving different regime for kinetic isotope fractionation. This means that identical clay mineralogy can be characterized by different Si isotope signatures depending on the geochemical conditions in which they were formed. Our results show that inheritance processes and the associated Si isotope signature of inherited clay minerals must be taken into account when using stable Si isotopes in terrestrial environments. This is in good agreement with recent findings showing that Si and Li isotope signatures of riverine sediments also integrate ancient and modern weathering processes (Zhang et al., 2017; Dellinger et al., 2017). The present study highlights the need to better understand how short-time and microscale soil processes, such as residence time of weathering solution in soil pore space, can affect dissolution/precipitation processes and the resulting Si isotope signature of clay minerals. This could also apply to microscale processes in pores of riverine and marine sediments. This is a time- and spatial-scale challenge allowing to better assess the controls of microscale physico-chemical processes in soils on variations of Si isotope signatures in land and oceans, as well land-ocean interfaces.

## Acknowledgments

We thank V. Lai and M. Soon (UBC) for assistance with element analysis and K. Gordon and J. Barling (UBC) for assistance with Si isotopic analysis. We thank M. Brzezinski (University of California Santa Barbara) for providing us diatomite. J-T.C. and S.O. were supported by “Fonds National de la Recherche Scientifique” of Belgium. This research was also supported by the ‘Soil Fertility Project’ within the Institutional Co-operation Programme between the Flemish Interuniversity Council (VLIR) and the Jimma University of Ethiopia, as well by D.W. NSERC Discovery Grant.

## References

Abraham, K., Opfergelt, S., Fripiat, F., Cavagna, A.-J., de Jong, J.T.M., Foley, S., André, L., Cardinal, D., 2008. $\delta^{30}$Si and $\delta^{29}$Si determinations on BHVO-1 and BHVO-2 reference materials via new configuration on Nu Plasma Multi Collector (MC)-ICP-MS. Geostand. Geoanal. Res. 32, 193–202.

Ameijeiras-Mariño, Y., Opfergelt, S., Schoonejans, J., Vanacker, V., Sonnet, P., De Jong, J., Delmelle, P., 2017. Impact of low denudation rates on soil chemical weathering intensity: a multiproxy approach. Chem. Geol. 456, 72–84.

Basile-Doelsch, I., Meunier, J.D., Parron, C., 2005. Another continental pool in the terrestrial silicon cycle. Nature 433, 399–402.

Bern, C.R., Brzezinski, M.A., Beucher, C., Ziegler, K., Chadwick, O.A., 2010. Weathering, dust, and biocycling effects on soil silicon isotope ratios. Geochim. Cosmochim. Acta 74, 876–889.

Berner, R.A., 1978. Rate control of mineral dissolution under earth surface conditions. Am. J. Sci. 278 (9), 1235–1252.

Bish, D.L., Von Dreele, R.B., 1989. Rietveld refinement of non-hydrogen atomic positions in kaolinite. Clay Clay Miner. 37, 289–296.

Bouchez, J., von Blanckenburg, F., Shuessler, J.A., 2013. Modeling novel stable isotope ratios in the weathering zone. Am. J. Sci. 313, 267–308.

Cardinal, D., Alleman, L.Y., De Jong, J., Ziegler, K., André, L., 2003. Isotopic composition of silicon measured by multicollector plasma source mass spectrometry in dry plasma mode. J. Anal. Atom. Spectrom. 18, 213–218.

Cardinal, D., Gaillardet, J., Hughes, H.J., Opfergelt, S., André, L., 2010. Contrasting silicon isotope signatures in rivers from the Congo Basin and the specific behaviour of organic-rich waters. Geophys. Res. Lett. 37, L12403.

Carpentier, M., Weis, D., Chauvel, C., 2013. Large U loss during weathering of upper continental crust: the sedimentary record. Chem. Geol. 340, 91–104.

Chadwick, O.A., Chorover, J., 2001. The chemistry of pedogenic thresholds. Geoderma 100, 321–353.

Christensen, B.T., 1992. Physical fractionation of soil and organic matter in primary particle size and density separates. In: Advances in Soil Science. Springer, pp. 1–90.

Cornelis, J.-T., Delvaux, B., Cardinal, D., André, L., Ranger, J., Opfergelt, S., 2010. Tracing mechanisms controlling the release of dissolved silicon in forest soil solutions using Si isotopes and Ge/Si ratios. Geochim. Cosmochim. Acta 74, 3913–3924.

Cornelis, J.-T., Delvaux, B., Georg, R.B., Lucas, Y., Ranger, J., Opfergelt, S., 2011. Tracing the origin of dissolved silicon transferred from various soil–plant systems towards rivers: a review. Biogeosciences 8, 89–112.

Cornelis, J.T., Weis, D., Lavkulich, L., Vermeire, M.-L., Delvaux, B., Barling, J., 2014a. Silicon isotopes record dissolution and reprecipitation of pedogenic clay minerals in a podzolic soil chronosequence. Geoderma 235–236, 19–29.

Cornelis, J.-T., Dumon, M., Tolossa, A.R., Delvaux, B., Deckers, J., Van Ranst, E., 2014b. The effect of pedological conditions on the sources and sinks of silicon in the Vertic Planosols in south-western Ethiopia. Catena 112, 131–138.

Dellinger, M., Bouchez, J., Gaillardet, J., Faure, L., Moureau, J., 2017. Tracing weathering regimes using the lithium isotope composition of detrital sediments. Geology 45, 411–414.

Delstanche, S., Opfergelt, S., Cardinal, D., Elsass, F., André, L., Delvaux, B., 2009. Silicon isotopic fractionation during adsorption of aqueous monosilicic acid onto iron oxide. Geochim. Cosmochim. Acta 73, 923–934.

Derry, L.A., Kurtz, A.C., Ziegler, K., Chadwick, O.A., 2005. Biological control of terrestrialsilica cycling and export fluxes to watersheds. Nature 433, 728–731.

Doebelin, N., Kleeberg, R., 2015. Profex: a graphical user interface for the Rietveld refinement program BGMN. J. Appl. Crystallogr. 48, 1573–1580.

Dumon, M., Tolossa, A.R., Capon, B., Detavernier, C., Van Ranst, E., 2014. Quantification of clay mineralogy of a Vertic Planosol in southwestern Ethiopia: impact on soil formation hypotheses. Geoderma 214, 184–196.

Engström, E., Rodushkin, I., Baxter, D.C., Öhlander, B., 2006. Chromatographic purification for the determination of dissolved silicon isotopic compositions in natural waters by high-resolution multicollector inductively coupled plasma mass spectrometry. Anal. Chem. 78, 250–257.

Frings, P.J., Clymans, W., Fontorbe, G., De La Rocha, C.L., Conley, D.J., 2016. The continental Si cycle and its impact on the ocean Si isotope budget. Chem. Geol. 425, 12–36.

Froelich, P.N., Andreae, M.O., 1981. The marine geochemistry of germanium: ekasilicon. Science 213, 205–207.

Geilert, S., Vroon, P.Z., Keller, N.S., Gudbrandsson, S., Stefánsson, A., 2015. Silicon isotope fractionation during silica precipitation from hot-spring waters: evidence from the Geysir geothermal field, Iceland. Geochim. Cosmochim. Acta 164, 403–427.

Georg, R.B., Reynolds, B.C., Frank, M., Halliday, A.N., 2006. New sample preparation techniques for the determination of Si isotopic compositions using MC-ICPMS. Chem. Geol. 235, 95–104.

Georg, R.B., Reynolds, B.C., West, A.J., Burton, K.W., Halliday, A.N., 2007. Silicon isotope variations accompanying basalt weathering in Iceland. Earth Planet. Sci. Lett. 261, 476–490.

Georg, R.B., Zhu, C., Reynolds, B.C., Halliday, A.N., 2009. Stable silicon isotopes of groundwater, feldspars, and clay coatings in the Navajo Sandstone aquifer, Black Mesa, Arizona, USA. Geochim. Cosmochim. Acta 73, 2229–2241.

Herbauts, J., Dehalu, F.A., Gruber, W., 1994. Quantitative determination of plant opal content in soils using a combined method of heavy liquid separation and alkali dissolution. Eur. J. Soil Sci. 45, 379–385.

IUSS Working Group WRB, 2015. World Reference Base for Soil Resources 2014. World Soil Resources Reports 106. FAO, Rome.

Kelly, E.F., 1990. Methods for extracting opal phytoliths from soil and plant material. In: Workshop on Biotic Indicators of Global Change, Seatlle, Washington.

Kleeberg, R., Monecke, T., Hillier, S., 2008. Preferred orientation of mineral grains in sample mounts for quantitative XRD measurements: how random are powder samples? Clay Clay Miner. 56, 404–415.

Kurtz, A.C., Derry, L.A., Chadwick, O.A., 2002. Germanium–silicon fractionation in the weathering environment. Geochim. Cosmochim. Acta 66, 1525–1537.

Jochum, K.P., Nohl, U., Herwig, K., Lammel, E., Stoll, B., Hofmann, A.W., 2005. GeoReM: a New Geochemical Database for Reference Materials and Isotopic Standards. Geostand. Geoanal. Res. 29, 333–338.

Lasaga, A.C., 1984. Chemical-kinetics of water–rock interactions. J. Geophys. Res. 89 (NB6), 4009–4025.

Lugolobi, F., Kurtz, A.C., Derry, L.A., 2010. Germanium–silicon fractionation in a tropical, granitic weathering environment. Geochim. Cosmochim. Acta 74, 1294–1308.

Maher, K., 2010. The dependence of chemical weathering rates on fluid residence time. Earth Planet. Sci. Lett. 294, 101–110.

Mehra, O.P., Jackson, M.L., 1960. Iron Oxides Removal From Soils and Clays by Dithionite Citrate System Buffered With Sodium Bicarbonate. Clays and Clay Minerals. Proc. 7th. Pergamon Press, London, pp. 317–327.

Mortlock, R.A., Froelich, P.N., 1996. Determination of germanium by isotope dilution-hydride generation inductively coupled plasma mass spectrometry. Anal. Chim. Acta 322, 5638–5645.

Oelze, M., von Blanckenburg, F., Hoellen, D., Dietzel, M., Bouchez, J., 2014. Si stable isotope fractionation during adsorption and the competition between kinetic and equilibrium isotope fractionation: implications for weathering systems. Chem. Geol. 380, 161–171.

Oelze, M., von Blanckenburg, F., Bouchez, J., Hoellen, D., Dietzel, M., 2015. The effect of Al on Si isotope fractionation investigated by silica precipitation experiments. Chem.

Geol. 397, 94–105.
Opfergelt, S., Delmelle, P., 2012. Silicon isotopes and continental weathering processes: assessing controls on Si transfer to the ocean. Compt. Rendus Geosci. 344, 723–738.
Opfergelt, S., Cardinal, D., André, L., Delvigne, C., Bremond, L., Delvaux, B., 2010. Variations of $\delta^{30}$Si and Ge/Si with weathering and biogenic input in tropical basaltic ash soils under monoculture. Geochim. Cosmochim. Acta 74, 225–240.
Opfergelt, S., Georg, R.B., Burton, K.W., Guicharnaud, R., Siebert, C., Gislason, S.R., Halliday, A.N., 2011. Silicon isotopes in allophane as a proxy for mineral formation in volcanic soils. Appl. Geochem. 26, S115–S118.
Opfergelt, S., Georg, R.B., Delvaux, B., Cabidoche, Y.M., Burton, K.W., Halliday, A.N., 2012. Silicon isotopes and the tracing of desilication in volcanic soil weathering sequences, Guadeloupe. Chem. Geol. 326–327, 113–122.
Opfergelt, S., Cornelis, J.-T., Houben, D., Givron, C., Burton, K.W., Mattielli, N., 2017a. The influence of weathering and soil organic matter on Zn isotopes in soils. Chem. Geol. 446, 140–148.
Opfergelt, S., Williams, H.M., Cornelis, J.-T., Guicharnaud, R.A., Georg, R.B., Siebert, C., Gislason, S.R., Halliday, A.N., Burton, K., 2017b. Iron and silicon isotope behavior accompanying weathering in Icelandic soils, and the implications for iron export from peatlands. Geochim. Cosmochim. Acta 217, 273–291.
Pogge von Strandmann, P.A.E., Opfergelt, S., Lai, Y.-J., Sigfusson, B., Gislason, S.R., Burton, K., 2012. Lithium, magnesium and silicon isotope behavior accompanying weathering in a basaltic soil and pore water profile in Iceland. Earth Planet. Sci. Lett. 339, 11–23.
Poitrasson, F., Viers, J., Martin, F., Braun, J.-J., 2008. Limited iron isotope variations in recent lateritic soils from Nsimi, Cameroon: implications for the global Fe geochemical cycle. Chem. Geol. 253, 54–63.
Pretorius, W., Weis, D., Williams, G., Hanano, D., Kieffer, B., Scoates, J., 2006. Complete trace elemental characterization of granitoid (USGS G-2, GSP-2) reference materials by high resolution inductively coupled plasma-mass spectrometry. Geostand. Geoanal. Res. 30, 39–54.
Reynolds, B.C., 2011. In: Baskaran, M. (Ed.), Handbook of Environmental Isotope Geochemistry, Advances in Isotope Geochemistry. Springer-Verlag Berlin Heidelberg, pp. 2011. https://doi.org/10.1007/978-3-642-10637-8_6.
Reynolds, B.C., Aggarwal, J., André, L., Baxter, D., Beucher, C., Brzezinski, M.A., Engström, E., Georg, B., Land, M., Leng, M.J., Opfergelt, S., Rodushkin, I., Sloane, H.J., Van den Boorn, S.H.J.M., Vroon, P.Z., Cardinal, D., 2007. An inter-laboratory comparison of Si isotope reference materials. J. Anal. Atom. Spectrom. 22, 561–568.
Roerdink, D.L., van den Boorn, S.H.J.M., Geilert, S., Vroon, P.Z., van Bergen, M.J., 2015. Experimental constraints on kinetic and equilibrium silicon isotope fractionation during the formation of non-biogenic chert deposits. Chem. Geol. 402, 40–51.
Sauer, D., Saccone, L., Conley, D.J., Herrmann, L., Sommer, M., 2006. Review of methodologies for extracting plant available and amorphous Si from soils and aquatic sediments. Biogeochemistry 80, 89–108.
Savage, P.S., Georg, R.B., Williams, H.M., Turner, S., Halliday, A.N., Chappell, B.W., 2012. The silicon isotope composition of granites. Geochim. Cosmochim. Acta 92, 184–202.
Scarlett, N.V.Y., Madsen, I.C., 2006. Quantification of phases with partial or no known crystal structures. Powder Diffract. 21, 278–284.
Schudel, G., Lai, V., Gordon, K., Weis, D., 2015. Trace element characterization of USGS reference materials by HR-ICP-MS and Q-ICP-MS. Chem. Geol. 410, 223–236.
Scribner, A.M., Kurtz, A.C., Chadwick, O.A., 2006. Germanium sequestration by soil: targeting the roles of secondary clays and Fe-oxyhydroxides. Earth Planet. Sci. Lett. 243, 760–770.
Stamm, F.M., Zambardi, T., Chmeleff, J., Schott, J., von Blanckenburg, F., Oelkers, E., 2019. The experimental determination of equilibrium Si isotope fractionation factors among $H_4SiO_4^o$, $H_3SiO_4$, and amorphous silica ($SiO_2$.0.32 $H_2O$) at 25 and 75°C using the three-isotope method. Geochim. Cosmochim. Acta 255, 49–68.
Steinhoefel, G., Breuer, J., von Blanckenburg, F., Horn, I., Kaczorek, D., Sommer, M., 2011. Micrometer silicon isotope diagnostics of soils by UV femtosecond laser ablation. Chem. Geol. 286, 280–289.
Sverdrup, H., 1996. Geochemistry, the key to understanding environmental chemistry. Sci. Total Environ. 183, 67–87.
Tadesse, S., Milesi, J.P., Deschamps, Y., 2003. Geology and mineral potential of Ethiopia: a note on geology and mineral map of Ethiopia. J. Afr. Earth Sci. 36, 273–313.
Ufer, K., Roth, G., Kleeberg, R., Stanjek, H., Dohrmann, R., Bergmann, J., 2004. Description of X-ray powder pattern of turbostratically disordered layer structures with a Rietveld compatible approach. Z. Krist.-Crystal. Mater. 219, 519–527.
Urey, H.C., 1947. The thermodynamic properties of isotopic substances. J. Chem. Soc. 562–581.
Van Ranst, E., Dumon, M., Tolossa, A.R., Cornelis, J.T., Stoops, G., Vandenberghe, R.E., Deckers, J., 2011. Revisiting ferrolysis processes in the formation of planosols for rationalizing the soils with stagnic properties in WRB. Geoderma 163, 265–274.
Vandevenne, F.I., Delvaux, C., Hughes, H., André, L., Ronchi, B., Clymans, W., Barao, L., Cornélis, J.-T., Govers, G., Meire, P., Struyf, E., 2015. Landscape cultivation alters $\delta^{30}$Si signature in terrestrial ecosystems. Sci. Rep. 5, 7732.
Wilson, S.A., 1997. Data Compilation for USGS Reference Material BHVO-2. U.S. Geological Survey Open-File Report, Hawaiian Basalt.
Zhang, X., Pringle, E., Dellinger, M., Bouchez, J., Gaillardet, J., Moynier, F., 2017. Silicon Isotopes in Large River Sediments: Imprint of Modern-Day Weathering vs. Continental Recycling. Goldschmidt conference Abstracts. vol. A. pp. 4496.
Ziegler, K., Chadwick, O.A., Brzezinski, M.A., Kelly, E.F., 2005. Natural variations of $\delta^{30}$Si ratios during progressive basalt weathering, Hawaiian Islands. Geochim. Cosmochim. Acta 69, 4597–4610.